Available online at www.sciencedirect.com
ScienceDirect
Journal of the European Ceramic Society 30 (2010) 1945–1954
www.elsevier.com/locate/jeurceramsoc

Particle size effect of starting SiC on processing, microstructures and mechanical properties of liquid phase-sintered SiC

Yoshihiro Hirata *, Naoto Suzue, Naoki Matsunaga, Soichiro Sameshima

Department of Chemistry, Biotechnology, and Chemical Engineering, Kagoshima University, 1-21-40 Korimoto, Kagoshima 890-0065, Japan

Received 7 October 2009; received in revised form 9 February 2010; accepted 27 February 2010
Available online 3 April 2010

Abstract

Dense SiC (97.3–99.2% relative density) of 1.1–3.5 μm average grain size was prepared by the combination of colloidal processing of bimodal SiC particles with sintering additives (Al_2O_3 plus Y_2O_3, 2–4 vol%) and subsequent hot-pressing at 1900–1950 °C. The fracture toughness of SiC was sensitive to the grain boundary thickness which was controlled by grain size and amount of oxide additives. A maximum fracture toughness (6.2 MPa $m^{1/2}$) was measured at 20 nm of grain boundary thickness. The mixing of 30 nm SiC (25 vol%) with 800 nm SiC (75 vol%) was effective to reduce the flaw size of fracture origin, in addition to a high fracture toughness, leading to the increase of flexural strength. However, the processing of a mixture of 30 nm SiC (25 vol%)–330 nm SiC (75 vol%) provided too small grains (1.1 μm average grain size), resultant thin grain boundaries (12 nm), decreased fracture toughness, and relatively large defect of fracture origin, resulting in the decreased strength.

Keywords: Hot-pressing; Strength; Toughness and toughening; SiC

1. Introduction

Densification of submicrometer-sized SiC particles is accelerated by dissolution–precipitation mechanism using SiO_2–Al_2O_3–Y_2O_3 liquid formed above 1400 °C.[1–7] The SiO_2 component is naturally formed on the surface of as-received SiC particles. In our previous studies,[7–9] the interaction of the SiC–Al_2O_3–R^{3+} ion system (R = Yb, Y, Gd, Sm, Nd and La) in an aqueous suspension was investigated to disperse a small amount of the sintering additives homogeneously on the surfaces of SiC particles. The consolidated SiC compacts were highly densified by hot-pressing at 1850–1950 °C.[5–7,9] On the other hand, it was found that the infiltration of a small amount of polytitanocarbosilane (PTC, precursor of SiC fiber) into a SiC green compact with Al_2O_3–Y_2O_3 additives increases the sinterability, flexural strength and fracture toughness of the hot-pressed SiC and suppresses the grain growth.[10–12] Similarly, it has been shown that the addition of 30 nm SiC to 800 nm SiC with Al_2O_3–Y_2O_3 additives decreases the grain growth and flaw size in the hot-pressed SiC, and improves the flexural strength.[9,12,13] The maximum strength was higher than 1 GPa. After the oxidation at 1300 °C, the mechanical properties of SiC were further improved to 960 MPa of average strength and 8.3 of Weibull modulus.[14] This reason may be related to the decrease of size and shape factor of fracture origins near the SiC surfaces by the formation of SiO_2 layer. As reported above, a smaller SiC powder in a bimodal particle size system has a higher solubility in a SiO_2–Al_2O_3–Y_2O_3 liquid than a larger SiC powder, and improves the resultant mechanical properties. However, the relation between size ratio of starting bimodal particle size system and sintered microstructure or resultant mechanical properties is not clearly understood. In this paper, the microstructures and mechanical properties of dense SiC were compared for three SiC samples processed with (1) 800 nm SiC, (2) 75 vol% 800 nm SiC–25 vol% 30 nm SiC and (3) 75 vol% 330 nm SiC–25 vol% 30 nm SiC.

2. Experimental procedure

2.1. Forming of green compact

The following three kinds of SiC suspensions were consolidated into a rectangular shape by casting in a gypsum mold

* Corresponding author. Tel.: +81 99 285 8325; fax: +81 99 257 4742.
E-mail address: hirata@apc.kagoshima-u.ac.jp (Y. Hirata).

0955-2219/$ – see front matter © 2010 Elsevier Ltd. All rights reserved.
doi:10.1016/j.jeurceramsoc.2010.02.026

at room temperature. (1) α-SiC powder of median size 800 nm (SiC A)[a] was dispersed at 30 vol% solid in a 0.3 M-$Y(NO_3)_3$ aqueous solution including α-Al_2O_3[b] powder of median size 200 nm at pH 5.0. The volume ratio of the SiC/Al_2O_3/Y_2O_3 components was adjusted to 1/0.012/0.0094 (1/0.0145/0.0145 mass ratio, named as A compact). (2) A plasma CVD-processed SiC powder of median size 30 nm (SiC B)[c] was mixed with 800 nm SiC at the volume ratio of 1 to 3. The mixed powders were dispersed at 20 vol% solid in 0.3 M-$Y(NO_3)_3$ aqueous solution including α-Al_2O_3 powder and polyacrylic acid dispersant (PAA, average molecular weight 10,000) of 1.0 mg/m^2-SiC surface at pH 5.0. The SiC/Al_2O_3/Y_2O_3 volume ratio was controlled to 1/0.012/0.012 (1/0.0150/0.0186 mass ratio, named as M compact). (3) β-SiC powder of median size 330 nm (SiC C)[d] was mixed with 30 nm SiC at the volume ratio of 3 to 1. The mixed powders were dispersed at 17 vol% solid in 0.22 M-$Y(NO_3)_3$ aqueous solution including α-Al_2O_3 powder and PAA of 1.5 mg/m^2-SiC surface at pH 5.0. The SiC/Al_2O_3/Y_2O_3 volume ratio was controlled to 1/0.020/0.016 (1/0.0253/0.0251 mass ratio, named as N compact). The properties of aqueous suspensions of A and M compacts were already reported in our previous papers.[5,9,13]

The preparation conditions of above three kinds of SiC suspensions were adjusted based on (1) Al_2O_3/Y_2O_3 ratio of sintering additives, (2) amount of sintering additives, (3) specific surface area of SiC particles and (4) adsorption of Y^{3+} ions on PAA dispersant fixed on SiC particles. According to Omori and Takei,[1] the sinterability of SiC shows a maximum at the mass ratio of $Al_2O_3/Y_2O_3 \approx 50/50$. The Al_2O_3/Y_2O_3 ratios of the above suspensions were controlled to be close 50/50 mass ratio. On the other hand, the specific surface area of starting SiC particles is larger in the following order: SiC B > SiC C > SiC A. For a constant volume of sintering additives, the effective amount of the sintering additives per m^2 of SiC decreases for SiC particles with a higher specific surface area. In our previous experiment,[11,13] the critical minimum amount of sintering additives for full densification was estimated to be 2 mg (Al_2O_3 plus Y_2O_3) per m^2 of SiC. This condition is also satisfied with the prepared SiC suspensions. Furthermore, it was possible to make a fluid 30 vol% powder suspension when only SiC A particles were mixed with Al_2O_3 in a $Y(NO_3)_3$ solution. However, it was difficult to make a fluid 20 vol% SiC suspension of mixed powder systems including fine 30 nm SiC particles (25 vol% SiC B).[11,13] PAA addition decreased the apparent viscosity of the mixed powder suspensions, indicating that the dispersibility of the nanometer-sized SiC particles was increased by the adsorption of PAA. PAA [(–CH_2–CH(COOH)–)$_n$] dissociates to produce negatively charged polymer and H^+ ions at pH higher than 3.[15] The negatively charged polymer is adsorbed on the positively charged $SiOH_2^+$ sites of SiC surfaces. When Y^{3+} ions and PAA are added to an SiC suspension, competitive adsorption of the two species onto the surface of SiC proceeds in addition to the interaction between Y^{3+} ions and PAA fixed to SiC particles.[6,8] That is, the amount of Y_2O_3 additive depends on the concentrations of $Y(NO_3)_3$ and PAA in the SiC suspension. Owing to the above reasons, different preparation conditions were designed for A, M and N compacts.

2.2. Hot-pressing and mechanical properties of SiC

The consolidated green compacts were hot-pressed under a pressure of 39 MPa at 1950 °C (A and M compacts) and at 1900 °C (N compact) for 2 h in an Ar flow (FVH-5: Fuji Dempa Kogyo Co., Ltd., Japan). In our previous experiment,[16] densification process using hot-pressing was measured in a temperature range from 1600 to 2050 °C for the SiC compacts consolidated with Al_2O_3–Y_2O_3 additives from colloidal SiC suspensions. Highly densified SiC was prepared at 1800–1950 °C of hot-pressing. To compare the microstructures of dense SiC in the above temperature range, the SiC A and M compacts including 800 nm SiC particles were hot-pressed at 1950 °C. On the other hand, the hot-pressing temperature of SiC N compact including 330 nm SiC particles was reduced to 1900 °C to achieve smaller SiC grains. The densities of the hot-pressed compacts were measured by the Archimedes method with double distilled water. The hot-pressed SiC was cut into the specimens with sizes of 3 mm height, 4 mm width, and 38 mm length, and polished with diamond paste of 1 μm. The flexural strength of hot-pressed SiC was measured at room temperature by four-point flexural method over spans of 30 mm (lower span) and 10 mm (upper span) at a crosshead speed of 0.5 mm/min. The fracture toughness was evaluated by single-edge V-notch beam (SEVNB) method. A thin diamond blade of 1 mm thick, where the tip of the V-notch had a curvature radius of 20 μm, was used to introduce a V-notch of $a/W = 0.1$–0.6 (a: notch length, W: width of the beam). The strengths of the notched specimens were measured by three-point loading over a span of 30 mm at a crosshead speed of 0.5 mm/min. Eq. (1) provides the fracture toughness for the SEVNB method and Eq. (2) indicates the shape factor (Y) of the crack at $S/W = 7.5$. S, P, and B in Eqs. (1) and (2) are the span width, applied load, and thickness of beam, respectively.

$$K_{IC} = \frac{3PS}{2BW^2} Y\sqrt{a} \tag{1}$$

$$Y = 1.964 - 2.837\lambda + 13.711\lambda^2 - 23.250\lambda^3 + 24.129\lambda^4 \quad \left(\lambda = \frac{a}{W}\right) \tag{2}$$

The phases formed on the surface of SiC were identified by X-ray diffraction (RINT 2200PCH/KG, Rigaku Co., Japan). The microstructures of SiC were observed by a scanning electron

[a] Chemical composition (mass%), SiC 98.90, SiO_2 0.66, C 0.37, true density 3.23 g/cm^3, specific surface area 13.4 m^2/g, Yakushima Electric Industry Co., Ltd., Kagoshima, Japan.

[b] Al_2O_3 > 99.99 mass%, specific surface area 10.5 m^2/g, Sumitomo Chemical Industry Co., Ltd., Tokyo, Japan.

[c] Chemical composition (mass%), SiC 95.26, SiO_2 0.97, C 3.76, true density 3.10 g/cm^3, specific surface area 50.4 m^2/g, Sumitomo Osaka Cement Co., Ltd., Tokyo, Japan.

[d] Chemical composition (mass%), SiC 97.35, SiO_2 0.29, C 2.13, true density 3.17 g/cm^3, specific surface area 18.5 m^2/g, Ibiden Co., Ltd., Gifu, Japan.

microscope (XL30, Japan FEI, Japan). The Young's modulus (E) was measured from the slope of the stress–strain curve. The fracture energy (γ) was calculated from the fracture toughness and Young's modulus as follows:

$$\gamma = \frac{K_{IC}^2}{2E} \quad (3)$$

3. Results and discussion

3.1. Preparation of bimodal SiC particle suspension (N compact)

Fig. 1 shows the zeta potential of SiC A (800 nm), SiC B (30 nm), SiC C (330 nm) and Al_2O_3 particles as a function of pH. The isoelectric points of SiC A, B, C and Al_2O_3 were pH 2.8, 2.8, 4.5 and 8.6, respectively. The surfaces of SiC particles were coated by thin SiO_2 film.[17] At a pH below the isoelectric point, the number of positively charged $SiOH_2^+$ sites becomes greater than that of negatively charged SiO^- sites. The opposite case occurs at a pH above the isoelectric point. Similarly, the number of $AlOH_2^+$ sites becomes greater than that of AlO^- sites at a pH below the isoelectric point. Therefore, pH 5 was selected to make heterocoagulation of SiC–Al_2O_3 mixed particles by electrostatic attraction force. Y^{3+} ions were also adsorbed on the negatively charged SiC surface but no interaction was measured between Y^{3+} ions and positively charged Al_2O_3 particles.[7]

Fig. 2 shows the shear stress–shear rate relation for the suspension of 330 nm SiC–30 nm SiC–200 nm Al_2O_3–Y^{3+} ion system with PAA at pH 5. The addition of PAA in the range from 1.25 to 1.50 mg/m^2-SiC was effective to decrease the shear stress of SiC suspensions. PAA [(–CH_2–CH(COOH)–)$_n$] releases H^+ ions and changes to negatively charged polymer above pH 3. The fraction of dissociated PAA reaches 100% above pH 9.0.[15] The decreased shear stress with addition of PAA is due to the increased electrostatic repulsion of PAA adsorbed on SiC particles. Further addition of PAA

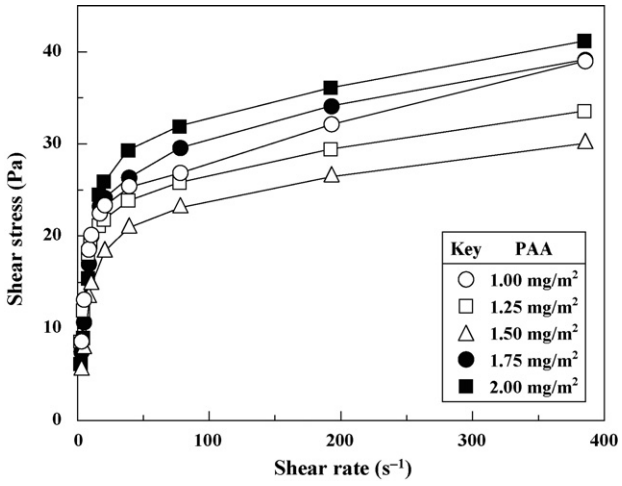

Fig. 2. Dependence of shear stress for 330 nm SiC (75 vol%)–30 nm SiC (25 vol%)–200 nm Al_2O_3–Y^{3+} ion system on the amount of PAA added.

(1.75 and 2.00 mg/m^2-SiC) increased again the shear stress. Coexistence of free PAA increases the ionic strength of the solution and compresses the electrical double layers, resulting in the decreased repulsive interaction between SiC particles with PAA.

Fig. 3 shows the amount of yttrium ions adsorbed on SiC particles in the suspensions at pH 5.0. The increased concentration of Y^{3+} ions increased the amount of Y^{3+} ions fixed on the SiC surface. This adsorption behavior of Y^{3+} ions was analyzed in our previous paper[8] and was represented by the Langmuir adsorption isotherm. As seen in Fig. 3, little difference was measured for the adsorption behavior of Y^{3+} ions between SiC B powder and SiC C powder. However, the bimodal particles system of 75 vol% SiC C–25 vol% SiC B with PAA (1.50 mg/m^2-SiC) showed higher amounts of Y^{3+} ions fixed. This phenomenon reflects the interaction between yttrium ions and PAA adsorbed on SiC surface. In this work, the concentration of $Y(NO_3)_3$ solution was adjusted to 0.22 mol/l to fix yttrium ions of 0.92 mg/m^2-SiC in the bimodal particle system.

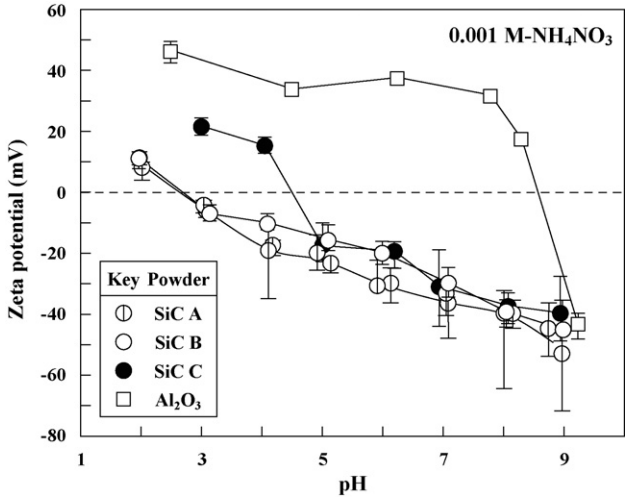

Fig. 1. Zeta potential of SiC A (800 nm), SiC B (30 nm), SiC C (330 nm) and Al_2O_3 particles as a function of pH.

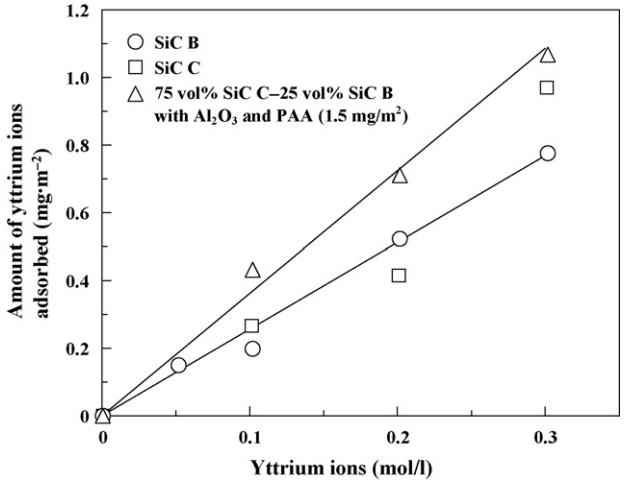

Fig. 3. Amount of yttrium ions adsorbed on SiC particles in the suspension at pH 5.

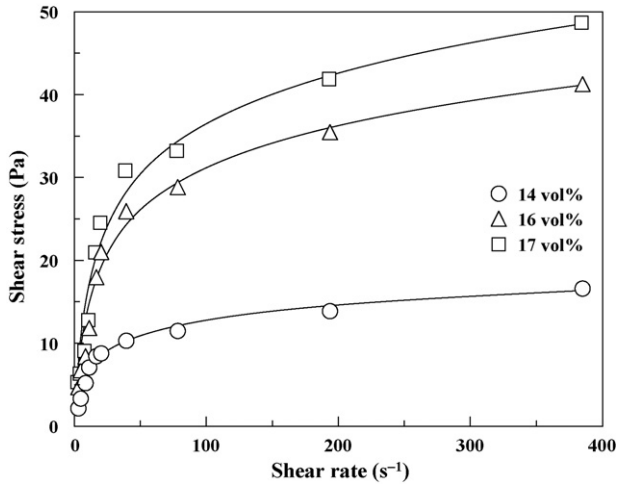

Fig. 4. Relationship between shear stress and shear rate for 14, 16 and 17 vol% solid suspensions of SiC–Al_2O_3–Y^{3+} ion system (N compact).

Fig. 4 shows the relationship between shear stress and shear rate for 14, 16 and 17 vol% solid suspensions of SiC–Al_2O_3–Y^{3+} ion system with 1.50 mg PAA/m^2-SiC. The shear stress of SiC suspensions was sensitive to the solid concentration and increased at a higher solid content of SiC. However, the green density after consolidation was almost constant (37.9–38.6% relative density). Further increase of the solid concentration to 20 vol% increased significantly the viscosity and decreased the green density to 35.7%. Therefore, 17 vol% solid suspension was used to make green compacts for hot-pressing. Similar experiments were done for the suspensions A and M compacts in previous papers[5,9,13] and the adequate preparation conditions are reported in Section 2.1.

3.2. Hot-pressing of SiC compacts

Fig. 5 shows the densification of SiC compacts during hot-pressing at 39 MPa. The green density of A compact (53.3%) decreased with addition of 25 vol% SiC B (30 nm) to 35.7% theoretical density (M compact) which was comparable to the green density (38.6% theoretical density) of 75 vol% SiC C–25 vol% SiC B system (N compact). This result suggests that the packing properties of finer SiC particles (SiC B) affect greatly the green density of the bimodal particles system.[18] The densification of A compact started at 1420 °C, which was close to the liquid formation temperature (≈1400 °C) at a given composition of the SiO_2–Al_2O_3–Y_2O_3 system.[19] Compared with A compact, M and N compacts began to shrink around 1000 °C. A possible explanation for the early densification in M and N compacts is the sintering between Al_2O_3–Al_2O_3 particles because the sizes of Al_2O_3 particles (200 nm) are larger than that of SiC B particles and preferred contact between Al_2O_3–Al_2O_3 particles is formed. After 2 h of hot-pressing at 39 MPa, all the compacts were densified above 97% theoretical density (97.3 ± 1.3% for A compact, 97.7 ± 1.5% for M compact, 99.2 ± 1.0% for N compact). According to previous experiments,[16] SiC A powder with Al_2O_3–Y_2O_3 additives were hot-pressed above 96% of theoretical density at 1800–1950 °C. The decrease of size of starting powder in N compact promoted more the densification than A and M compacts at a low temperature.

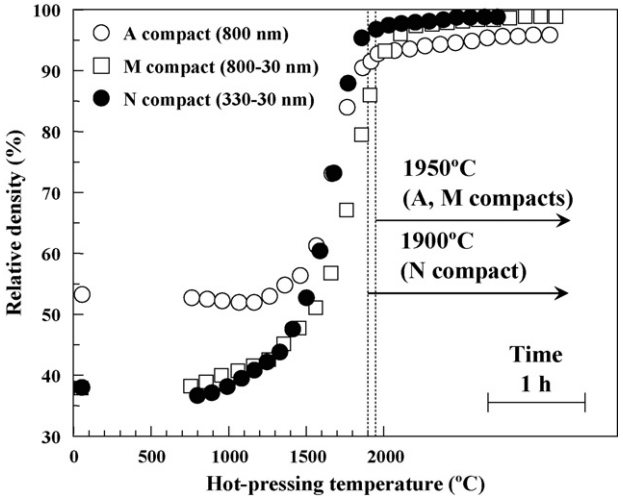

Fig. 5. Densification curves of SiC compacts during the hot-pressing at 39 MPa.

3.3. Microstructures of SiC compacts

Fig. 6 shows the X-ray diffraction patterns of SiC compacts hot-pressed at 1900 or 1950 °C. The as-hot-pressed SiC A and M consisted of 6H- and 33R-type SiC. The 6H- and 33R-SiC phases were contained in 800 nm SiC powder. After the hot-pressing, 15R-SiC was also identified in A and M compacts. SiC N compacts contained 3C-SiC which was included in 30 and 330 nm SiC powders. Crystalline $Y_2O_3{\cdot}Al_2O_3$ and $3Y_2O_3{\cdot}5Al_2O_3$ were identified in all the SiC compacts, suggesting that these oxides were formed at grain boundaries from the liquid containing SiC during the cooling process. According to the phase diagram of SiO_2–Y_2O_3–Al_2O_3 sys-

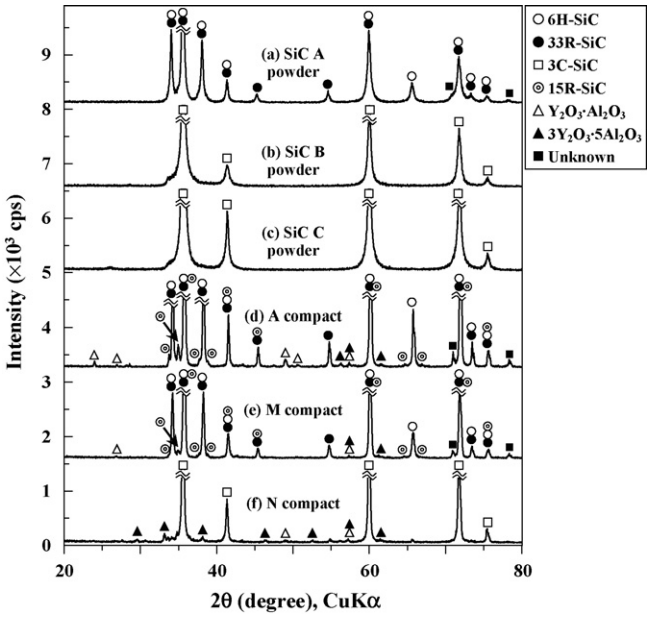

Fig. 6. X-ray diffraction patterns of SiC A powder (a), SiC B powder (b), SiC C powder (c), A compact (d), M compact (e) and N compact (f) hot-pressed.

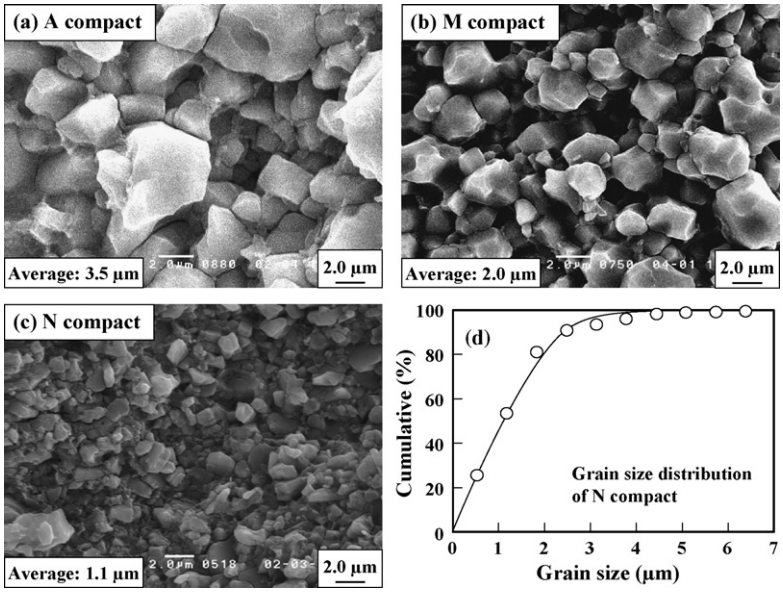

Fig. 7. Microstructures of (a) A, (b) M and (c) N compacts hot-pressed at 1950 °C (a, b) and 1900 °C (c). (d) The grain size distribution of N compact.

tem for the composition of N compact, a liquid is formed above 1750 °C, which dissolves nanometer-sized SiC particles. During the cooling process, $3Y_2O_3{\cdot}5Al_2O_3$ is precipitated as a primary crystal at 1750 °C. Further cooling from 1750 to 1450 °C, Al_2O_3 crystallizes from the liquid together with $3Y_2O_3{\cdot}5Al_2O_3$ (liq.–$3Y_2O_3{\cdot}5Al_2O_3$–Al_2O_3 system). At about 1400 °C, $2Y_2O_3{\cdot}3SiO_2$ crystallizes from the liquid to form three phases of Al_2O_3–$3Y_2O_3{\cdot}5Al_2O_3$–$2Y_2O_3{\cdot}3SiO_2$ system. A similar analysis of crystallization of sintering additives is possible for M compact. The final phases of A compact cooled to 1400 °C are Al_2O_3–$2Y_2O_3{\cdot}3Al_2O_3$–$3Al_2O_3{\cdot}2SiO_2$ system. During the cooling process, SiC is also precipitated from the liquid (Fig. 9). However, temperature dependence of the solubility of SiC in the liquid is not well understood.[20] As seen in Fig. 6, $Y_2O_3{\cdot}Al_2O_3$ and $3Y_2O_3{\cdot}5Al_2O_3$ were observed after the hot-pressing at 1900–1950 °C. The compound $3Y_2O_3{\cdot}5Al_2O_3$ is produced above 1400 °C in the phase diagram but $Y_2O_3{\cdot}Al_2O_3$ is a metastable phase at a given additive composition. No mullite or no Y_2O_3–SiO_2 compound was observed by the X-ray diffraction patterns in Fig. 6. That is, the above experimental result is in accordance with the reaction of two components of Y_2O_3–Al_2O_3 system rather than three components of SiO_2–Y_2O_3–Al_2O_3 system. The possible reaction is the preferred reaction between SiO_2 layer on SiC particles and excess carbon contained in SiC B and SiC C powder (2.1–3.8 mass%) to produce volatile compounds during hot-pressing: SiO_2 (s) + C (s) → SiO (g) + CO (g). Y_2O_3 and Al_2O_3 have lower reactivity with carbon than SiO_2. In a next paper, the detailed structure of grain boundary enriched with $Y_2O_3{\cdot}Al_2O_3$ and $3Y_2O_3{\cdot}5Al_2O_3$ may be investigated.

Fig. 7 shows the microstructures of SiC hot-pressed at 1900 and 1950 °C. The average grain size was 3.5, 2.0 and 1.1 μm for compacts A, M and N, respectively. Addition of 30 nm SiC to 800 nm SiC and to 330 nm SiC decreased the grain size as compared with the SiC from 800 nm SiC. The solubility of SiC (C_r) with a particle radius, r, in the oxide liquid at a given temperature (T) is expressed by Thomson–Freundlich equation,[21]

$$\ln\left(\frac{C_r}{C_0}\right) = \frac{2M\sigma}{kTr\rho} = \frac{2\sigma v}{kTr} \tag{4}$$

where C_0 is the solubility of SiC at $r \to \infty$, M the molecular weight of SiC, σ the interfacial energy at the interface between solid SiC and liquid, k the Boltzmann constant, ρ the density of SiC and v is the volume per SiC molecule. The solubility of the SiC increases exponentially with decreasing particle size. Above relationship proposes that 30 nm SiC particles dissolve faster than 330 or 800 nm SiC in the liquid, and precipitate on the surfaces of 330 and 800 nm SiC particles, respectively.

Fig. 8 shows the schematic concentration profile of SiC molecules in the liquid around SiC grain with size r. The flux (J) of SiC molecules from x (distance from the surface of 330 or 800 nm SiC grain) = ∞ to $x = 0$ is represented by Eqs. (5) and (6). Eqs. (5) and (6) express the diffusive and convective transport, and mass transport by diffusion without convention,

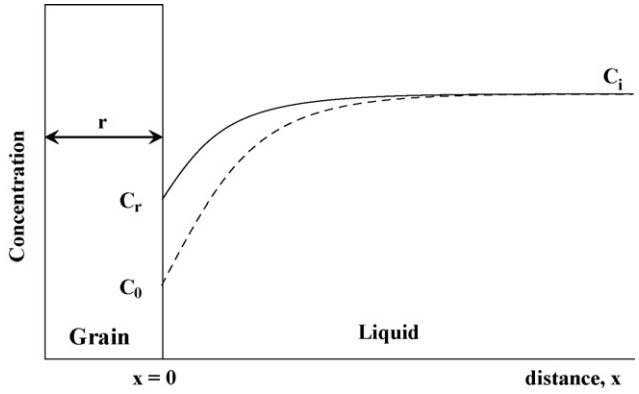

Fig. 8. Concentration profile of diffusing SiC molecules which control the growth rate of SiC.

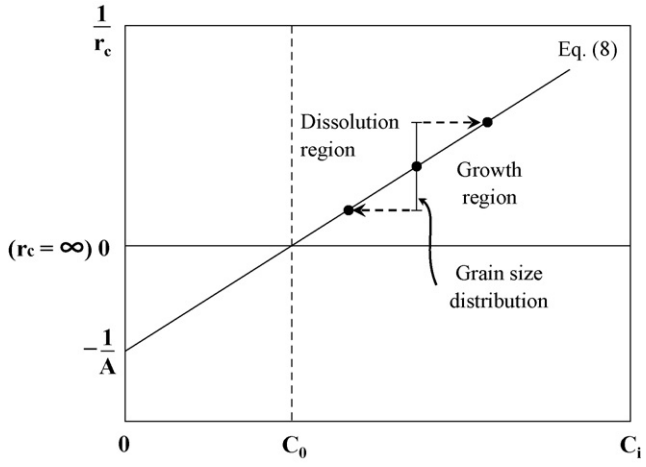

Fig. 9. Relation between critical radius of SiC grain and concentration of SiC molecules (C_i) in a solution (see Eq. (8) in text).

respectively.[22] The arriving SiC molecules are attached to 330 or 800 nm SiC surface, leading to the grain growth of SiC,

$$J = -\frac{D}{\delta}(C_i - C_r) = -(\rho - C_0)\frac{dr}{dt} \quad (5)$$

$$J = -\frac{D}{r}(C_i - C_r) = -(\rho - C_0)\frac{dr}{dt} \quad (6)$$

where C_i is the concentration of SiC molecules at $x = \infty$, C_r the surface concentration of diffusing SiC molecules, C_0 the equilibrium concentration for $r = \infty$, δ the effective diffusion layer thickness and t is reaction time. The difference of $C_r - C_0$ is expressed by Eq. (7) if the particles are not too small.

$$C_r - C_0 = C_0 \exp\left(\frac{2v\sigma}{kTr}\right) - C_0 \approx \frac{C_0 A}{r} \quad \left(A = \frac{2v\sigma}{kT}\right) \quad (7)$$

The condition of $dr/dt = 0$ for Eqs. (5) and (6) gives Eq. (8) for a dilute solution ($\rho - C_0 \approx \rho$),

$$\frac{1}{r_c} = \frac{C_i}{C_0 A} - \frac{1}{A} \quad (8)$$

where r_c is the critical radius of SiC grain corresponding to $dr/dt = 0$. Fig. 9 shows the relationship between $1/r_c$ and C_i. The grain size distribution is an important factor controlling the dissolution and precipitation rates. The grains larger than r_c grow by the precipitation of SiC molecules and the grains smaller than r_c shrink by the dissolution. As a result, the number of grains decreases because small grains dissolve and large grains grow, and a continuous increase in mean grain size occurs.

3.4. Mechanical properties of SiC compacts

3.4.1. Fracture toughness

Fig. 10 summarizes the mechanical properties of SiC compacts hot-pressed. The average strength of A compact (565 MPa) increased to 812 MPa by the addition of 30 nm SiC (M compact). On the other hand, the average strength of N compact (548 MPa) was comparable to that of A compact. The maximum

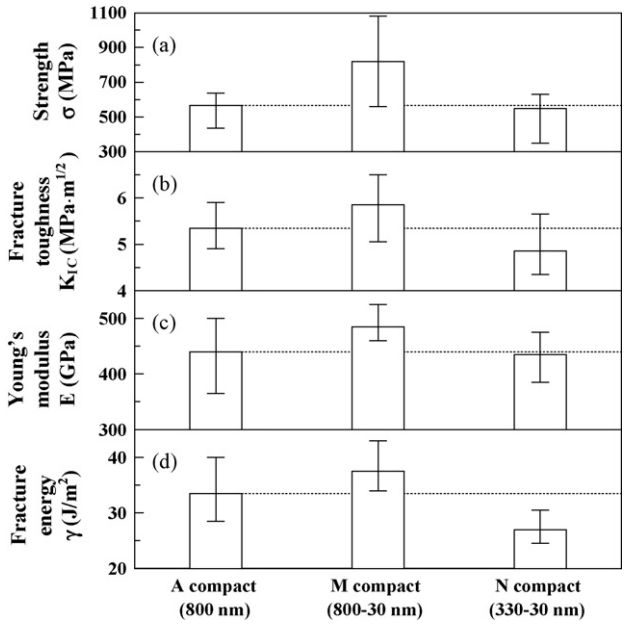

Fig. 10. Mechanical properties of SiC compacts hot-pressed at 1900–1950 °C.

strength was 637, 1080 and 632 MPa for A, M and N compacts, respectively. A similar tendency was also observed for fracture toughness, Young's modulus and fracture energy. Especially, the fracture toughness and fracture energy of N compact decreased as compared with A compact. This result is discussed in relation to the microstructures of dense SiC. The thickness (d) of sintering additives at grain boundary was calculated using the cubic model of SiC grain in Fig. 11. The volume ratio of sintering additives (v_{oxide}) to SiC grain (v_{SiC}) is represented by Eq. (9).

$$\frac{v_{oxide}}{v_{SiC}} = \frac{(r+2d)^3 - r^3}{r^3} = 6\left(\frac{d}{r}\right) + 12\left(\frac{d}{r}\right)^2 + 8\left(\frac{d}{r}\right)^3 \quad (9)$$

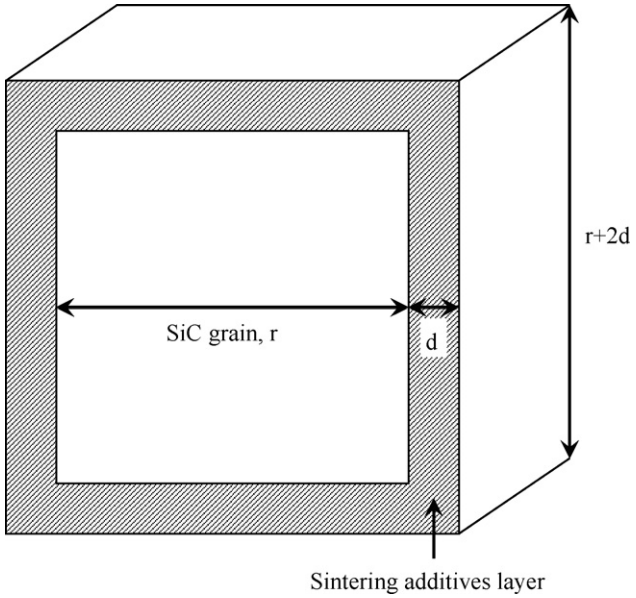

Fig. 11. Model structure of cubic SiC grain with sintering additive layer of thickness d.

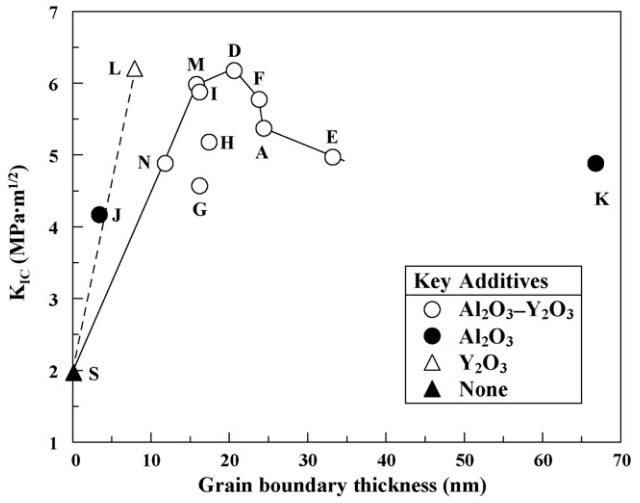

Fig. 12. Relationship between K_{IC} and calculated thickness of grain boundary of SiC hot-pressed. See Table 1 for samples.

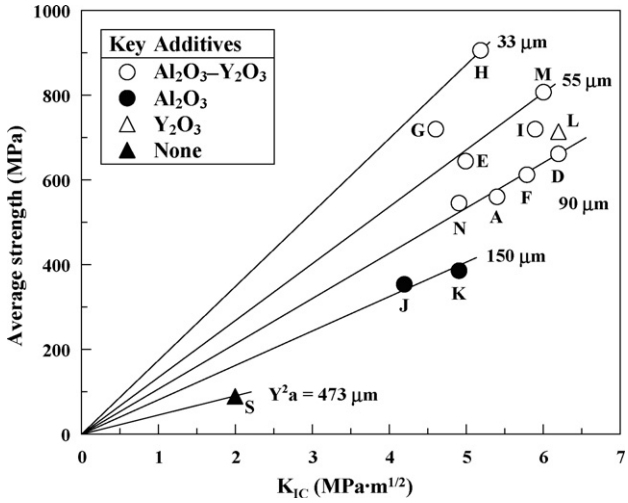

Fig. 13. Average strength and K_{IC} for SiC hot-pressed. See Table 1 for samples.

The grain boundary thickness ($2d$) of liquid phase-sintered SiC is approximated to be $2d = r(v_{oxide}/v_{SiC})/3$ under the condition of $d/r \ll 1$. Increased amount of sintering additives and grain growth of SiC lead to the formation of thick grain boundaries.

Table 1 shows the calculated thickness of grain boundary for dense SiC with Al_2O_3–Y_2O_3, Al_2O_3 and Y_2O_3 as sintering additives. In Table 1, the information of previously measured microstructures and mechanical properties are also presented.[9,16,17,20] Fig. 12 shows the relation between K_{IC} and calculated thickness of grain boundary. The SiC (800 nm) hot-pressed without sintering additives at 1800 °C (77% relative density) showed 2.0 MPa $m^{1/2}$ of fracture toughness.[23] The addition of a small amount of Al_2O_3, Y_2O_3 and Al_2O_3–Y_2O_3 oxides (0.2–4.5 vol%) improved significantly the densification of SiC at 1800–1950 °C (>96% theoretical density). The oxide-rich liquid dissolves SiC grain and the dissolved SiC molecules form strong chemical bonds between adjacent SiC grains during the precipitation process (Fig. 9). The remaining liquid is solidified as crystalline or amorphous phase during the cooling process to form strong bonds at grain boundaries. As seen in Fig. 7, cracks propagated along grain boundaries of SiC with Al_2O_3–Y_2O_3 additives. The K_{IC} in Fig. 12 reflects the fracture energy for grain boundaries of dense SiC. The increase of thickness of grain boundaries is accompanied by the increase of K_{IC}, indicating the formation of strong bonding at grain boundaries. The K_{IC} reaches a maximum at around 20 nm of grain boundary thickness. Too thick grain boundary enriched with oxide additives decreases K_{IC} value. This result may be explained by the decreased fracture energy due to the formation of oxide-rich chemical bonds. The difference of K_{IC} among A, M and N compacts is well understood by the thickness of grain boundary. As presented by Eq. (9), the grain boundary thickness ($2d$) corresponding to the maximum K_{IC} is controlled by grain size of SiC (r) and volume fraction of sintering additives (v_{oxide}). At a given v_{oxide}, significant grain growth of SiC leads to the relation $2d > 2d_0$ (maximum K_{IC}), resulting in the decreased K_{IC} (A

Table 1
Calculated thickness of grain boundary and the product of Y (shape factor) and a (size) of fracture origin for dense SiC with Al_2O_3–Y_2O_3, Al_2O_3 and Y_2O_3 as sintering additives.

Sample (hot-pressed temp.,°C)	Additives (vol%)		Grain size (μm)	Grain boundary thickness (nm)	K_{IC} (MPa $m^{1/2}$)	Strength (MPa)	Y^2a (μm)
	Al_2O_3	Y_2O_3					
A (1950)	1.2	0.94	3.5	24.4	5.4	565	91.3
D (1850)	1.2	0.94	2.9	20.5	6.2	666	86.7
E (1800)	2.0	1.6	2.8	33.2	5.0	647	59.7
F (1800)	2.0	1.6	2.0	23.7	5.8	615	88.9
M[a] (1950)	1.2	1.2	2.0	15.9	6.0	812	54.6
N[a] (1900)	2.0	1.6	1.0	11.8	4.9	548	80.0
G[a] (1950)	1.2	3.3	1.1	16.3	4.6	723	40.5
H[a,P] (1950)	1.2	1.2	2.2	17.5	5.2	911	32.5
I[P] (1950)	1.2	0.94	2.3	16.3	5.9	724	66.4
J (1950)	0.2	0	5.2	3.5	4.2	357	138.4
K (1850)	3.5	0	5.8	66.9	4.9	390	157.9
L (1950)	0	1.0	2.4	7.9	6.2	719	74.4
S (1800)	0	0	–	0	2.0	92	472.6

[a] Bimodal particles system, N: 330–30 nm, M, G, H: 800–30 nm, P: polytitanocarbosilane (PTC) was infiltrated. H: 3 vol% PTC, I: 1.3 vol% PTC.

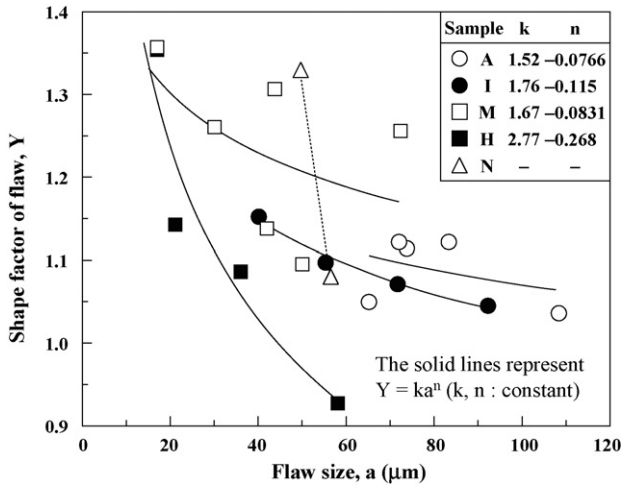

Fig. 14. Relationship between shape factor (Y) and flaw size (a) for A, H, I, M and N compacts.

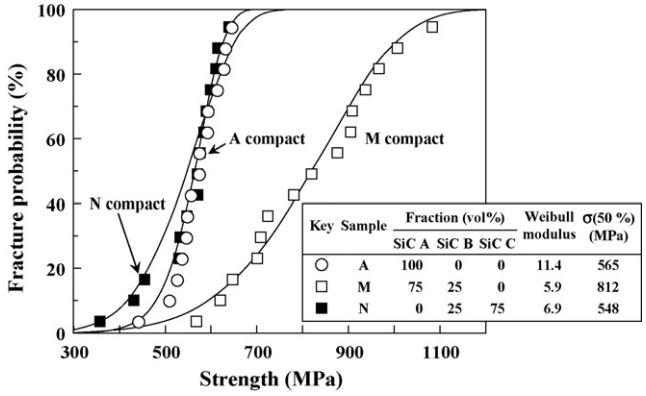

Fig. 15. Fracture probability for A, M and N compacts hot-pressed at 1900–1950 °C.

compact). Too suppression of grain growth of SiC provides the relation of $2d < 2d_0$ (maximum K_{IC}), resulting in the decreased K_{IC} (N compact). That is, K_{IC} of SiC is sensitive to the product of rv_{oxide} and reaches a maximum of $2d = 20$ nm for Al_2O_3 (1.2–2.0 vol%)–Y_2O_3 (0.94–1.6 vol%) additives. When sintering additive is different, the bonding energy at grain boundaries of SiC is changed. The influence of sintering additives on K_{IC} is seen in the data of J, K and L samples with only Al_2O_3 or Y_2O_3 additive in Fig. 12. The interesting result is the relatively high K_{IC} value for K sample with thick grain boundary. Generally, pressureless sintering of SiC needs more sintering additives than hot-pressing to produce dense products.[11] The decreased tendency of K_{IC} for Al_2O_3–Y_2O_3 additives in the range $2d > 20$ nm and K_{IC} for K sample indicate a nearly constant K_{IC} value for thick grain boundary.

3.4.2. Strength

According to fracture mechanic, the strength of ceramics (σ_f) is dominated by fracture toughness (K_{IC}), size (a) and shape factor (Y) of fracture origin (Eq. (10)).

$$\sigma_f = \frac{K_{IC}}{Y\sqrt{a}} \tag{10}$$

Table 1 and Fig. 13 summarize average strength and the product of Y^2a for SiC with Al_2O_3–Y_2O_3, Al_2O_3 and Y_2O_3 additives. The comparison of mechanical properties among A, M and N samples gives the following interpretation. (1) A slight decrease of strength from A to N compact is due to the decrease of K_{IC}. (2) The product Y^2a associated with the fracture origin is almost equal between A and N compacts. (3) The increased strength from A to M compact is explained by the increase of K_{IC} and decrease of Y^2a. Addition of 30 nm SiC particles to 330 nm SiC particles in N compact provided a high density after hot-pressing at 1900 °C but remained larger fracture origins than M compact

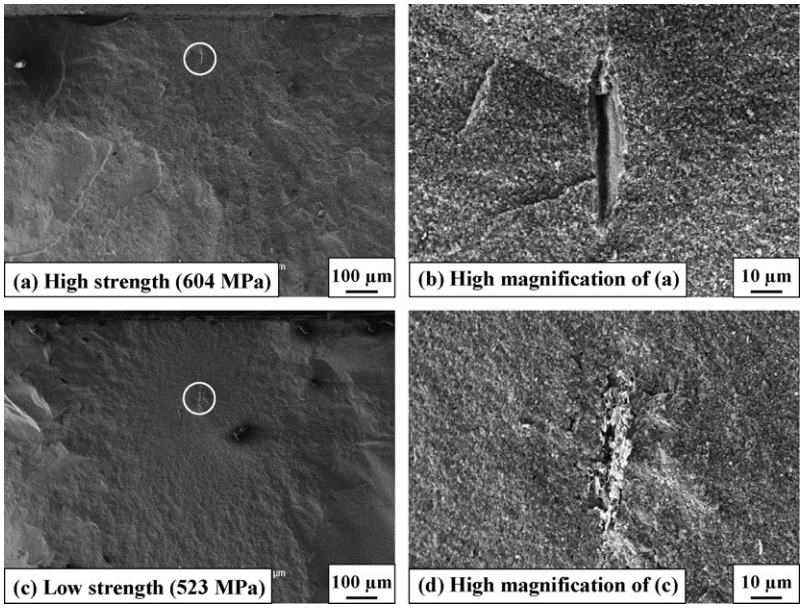

Fig. 16. Fracture origins observed in N compacts of strength of (a, b) 604 MPa and (c, d) 523 MPa.

where 30 nm SiC particles were mixed with 800 nm SiC particles. Further improvement of strength due to the decrease of Y^2a value was achieved by the addition of both polytitanocarbosilane (PTC, precursor of SiC fiber) and 30 nm SiC to 800 nm SiC (H sample). In our previous paper,[24] the relation between the addition of 30 nm SiC and a or Y value was investigated by observation of fracture origin of SiC hot-pressed. Fig. 14 shows the relation between shape factor and flaw size for A, H, I and M compacts and the following conclusions are derived: (1) Y value increases as a value decreases, (2) addition of PTC to SiC A compact decreases the flaw size with little change of Y value (I compact), (3) addition of SiC B to SiC A decreases the flaw size but Y value increases (M compact), (4) both the addition of PTC and SiC B to SiC A decreases flaw size and Y value (H compact).

Fig. 15 shows the fracture probability for SiC hot-pressed. The Weibull modulus was 11.4 for A compact, 5.9 for M compact and 6.9 for N compact, respectively. The small Weibull modulus for SiC M compact reflects the relatively wide range of flaw size and shape factor. The fracture probability of N compact in the range from 500 to 630 MPa (20% < fracture probability < 100%) was close to that of A compact. This result suggests that a similar distribution of Y^2a values was produced in both the hot-pressed SiC compacts (Fig. 13).

Fig. 16 shows the typical fracture origins of N compacts of high strength (a, b) and low strength (c, d). The flaw observed in Fig. 11(b) was 56 μm in size and had a sharp edge (Y = 1.08). On the other hand, the flaw observed in Fig. 11(d) is the porous region of about 50 μm length (Y = 1.32). The sizes of both fracture origins were relatively similar. These data are plotted in Fig. 14. The result for N compact suggests that (1) the addition of 30 nm SiC to 330 nm SiC decreases the flaw size as compared with A compact and (2) the range of Y value is comparable to that of M compact. Although more observation of fracture origins in N compacts is needed, the Weibull modulus may reflects mainly the distribution of Y value rather than a value.

4. Conclusions

(1) Y^{3+} ions were adsorbed on the negatively charged SiC particles at pH 5 and the amount of Y^{3+} ions adsorbed was controlled by the concentration of Y^{3+} ions.
(2) The addition of PAA in the range from 1.25 to 1.5 mg/m^2-SiC was effective to decrease the apparent viscosity. Coexistence of free PAA increased the ionic strength and increased the viscosity of suspension.
(3) The packing properties of finer SiC particles (∼30 nm) added to larger SiC particles (330 or 800 nm) affected greatly the green density of the bimodal particles system.
(4) The addition of Al_2O_3 plus Y_2O_3 of 2–4 vol% densified SiC above 97% relative density by hot-pressing at 1900–1950 °C.
(5) The fracture toughness of liquid phase-sintered SiC was very sensitive to the grain size and the amount of oxide additives. Too small grain or excess oxide additives decreased the fracture toughness (fracture energy) of SiC.
(6) The strength and Weibull modulus of SiC were closely related of the size (a) and shape factor (Y) of flaw in the range from 20 to 100 μm. The addition of 30 nm SiC to 800 nm SiC contributed to the decrease of flaw size, leading to the increased strength (maximum strength > 1 GPa). However, Weibull modulus was low (5.9) because of the wide range of a and Y values. The addition of 30 nm SiC to 330 nm SiC provided a higher Weibull modulus but the strength decreased because of the relatively large Y^2a value and low K_{IC}.

References

1. Omori M, Takei H. Pressureless sintering of SiC. *J Am Ceram Soc* 1982;**65**(6):C92.
2. Lange FF. Hot-pressing behavior of silicon carbide powders with additions of aluminium oxide. *J Mater Sci* 1975;**10**(2):314–20.
3. Mulla MA, Kristic VD. Low-temperature pressureless sintering of β-silicon carbide with aluminium oxide and yttrium oxide additions. *Am Ceram Soc Bull* 1991;**70**(3):439–43.
4. Wang XH, Hirata Y. Colloidal processing and mechanical properties of SiC with Al_2O_3 and Y_2O_3. *J Ceram Soc Jpn* 2004;**112**(1):22–8.
5. Hidaka N, Hirata Y. Colloidal processing and liquid phase sintering of SiC–Al_2O_3–Y^{3+} ions system. *Ceram Trans* 2004;**152**:109–18.
6. Tabata S, Hirata Y. Colloidal processing of SiC with 700 MPa of flexural strength. *Ceram Trans* 2004;**152**:119–28.
7. Hidaka N, Hirata Y, Sameshima S. Colloidal processing of the SiC–Al_2O_3–Y^{3+} ions system and sintering behavior of the consolidated powder compacts. *J Ceram Process Res* 2002;**3**(4):271–7.
8. Hirata Y, Tabata S, Ideue J. Interactions in the silicon carbide–polyacrylic acid–yttrium ion system. *J Am Ceram Soc* 2003;**86**(1):5–11.
9. Hidaka N, Hirata Y. Mixing effect of nanometer-sized SiC powder on processing and mechanical properties of SiC using submicrometer-sized powder. *J Ceram Soc Jpn* 2005;**113**(7):446–72.
10. Hidaka N, Hirata Y, Sameshima S, Sueyoshi H. Hot-pressing and mechanical properties of SiC ceramics with polytitanocarbosilane. *J Ceram Process Res* 2004;**5**(4):331–6.
11. Hirata Y, Matsunaga N, Hidaka N, Tabata S, Sameshima S. Processing of high performance silicon carbide. *J Ceram Soc Jpn* 2008;**116**(6):665–73.
12. Hirata Y, Matsunaga N, Hidaka N, Maeda T, Arima T, Sameshima S. Improvement of strength, Weibull modulus and damage tolerance of SiC. *Mater Sci Forum* 2007;**561–565**:489–94.
13. Hidaka N, Hirata Y. Sintering and mechanical properties of SiC using nanometer-size powder. In: *Proceedings of 6th pacific rim conference on ceramic and glass technology - Pac Rim 6 (CDR)*. The American Ceramic Society; 2006.
14. Matsunaga N, Nakahama K, Hirata Y, Sameshima S. Enhancement of strength of SiC by heat-treatment in air. *J Ceram Process Res* 2009;**10**(3):319–24.
15. Hirata Y, Kamikakimoto J, Nishimoto A, Ishihara Y. Interaction between alpha-alumina surface and polyacrylic-acid. *J Ceram Soc Jpn* 1992;**100**(1):7–12.
16. Hidaka N, Hirata Y, Wang XH, Tabata S. Aqueous processing, hot-pressing and mechanical properties of silicon carbide with Al_2O_3 with Y_2O_3. *J Ceram Soc Jpn* 2005;**113**(2):143–8.
17. Hirata Y, Hidaka K, Matsumura H, Fukushige Y, Sameshima S. Colloidal processing and mechanical properties of silicon carbide with alumina. *J Mater Res* 1997;**12**(11):3146–57.
18. Hirata Y, Shih WH.Proceedings of 9th CIMTEC – world ceramics congress, ceramics: getting into the 2000s – Part B. *Adv Sci Technol* 1999;**14**:637–44.
19. Levin EM, Robbins CR, McMurdie HF. In: Reser MK, editor. *Phase diagrams for ceramists, 1969 supplement (figures 2067–4149)*. Columbus, OH: The Am. Ceram. Soc.; 1969. p. 165 [Fig. 2586].

20. Tabata S, Hirata Y, Sameshima S, Matsunaga N, Ijichi K. Liquid phase sintering and mechanical properties of SiC with rare-earth oxide. *J Ceram Soc Jpn* 2006;**114**(3):247–52.
21. Swalin RA. *Thermodynamics of solid*. New York: John Wiley & Sons; 1972. p. 180–4.
22. Doremus RH. *Rates of phase transformations*. New York: Academic Press, Inc.; 1985, p.143–6.
23. Sameshima S, Miyano K, Hirata Y. Sinterability of SiC powder coated uniformly with Al ions. *J Mater Res* 1998;**13**(4):816–20.
24. Matsunaga N, Hidaka N, Sameshima S, Hirata Y. Mechanical properties of SiC processed with nanometer-sized powder and polytitanocarbosilane. *Key Eng Mater* 2007;**352**:73–6.